

Rate-dependent phase transformations in nanoindented germanium

D. J. Oliver, J. E. Bradby, J. S. Williams, M. V. Swain, and P. Munroe

Citation: [Journal of Applied Physics](#) **105**, 126101 (2009); doi: 10.1063/1.3151967

View online: <http://dx.doi.org/10.1063/1.3151967>

View Table of Contents: <http://scitation.aip.org/content/aip/journal/jap/105/12?ver=pdfcov>

Published by the [AIP Publishing](#)

Articles you may be interested in

[Phase transformation pathways in amorphous germanium under indentation pressure](#)

J. Appl. Phys. **115**, 153502 (2014); 10.1063/1.4871190

[Nanoindentation experiments with different loading rate distinguish the mechanism of incipient plasticity](#)

Appl. Phys. Lett. **103**, 072101 (2013); 10.1063/1.4818260

[Effect of hydrogen on nanoindentation-induced phase transformations in amorphous silicon](#)

J. Appl. Phys. **106**, 123511 (2009); 10.1063/1.3267853

[Nanoindentation-induced phase transformation in relaxed and unrelaxed ion-implanted amorphous germanium](#)

J. Appl. Phys. **106**, 093509 (2009); 10.1063/1.3255999

[Indentation-induced crystallization and phase transformation of amorphous germanium](#)

J. Appl. Phys. **96**, 1464 (2004); 10.1063/1.1766414



Re-register for Table of Content Alerts

Create a profile.



Sign up today!



Rate-dependent phase transformations in nanoindented germanium

D. J. Oliver,^{1,a)} J. E. Bradby,¹ J. S. Williams,¹ M. V. Swain,² and P. Munroe³

¹Department of Electronic Materials Engineering, Research School of Physics and Engineering, The Australian National University, Canberra, Australia's Capital Region 0200, Australia

²Biomaterials Science Research Unit, Faculty of Dentistry, The University of Sydney, Eveleigh, New South Wales 1430, Australia

³Electron Microscope Unit, University of New South Wales, Sydney, New South Wales 2052, Australia

(Received 6 March 2009; accepted 11 May 2009; published online 17 June 2009)

There is considerable controversy over the deformation behavior of germanium (Ge) under nanoindentation using a sharp diamond tip, with a diverse range of observations that suggest competing mechanisms. Here we show the deformation mechanism of Ge can be controlled by the rate of applied load. Loading rate is varied over three orders of magnitude using depth-sensing nanoindentation. At slow loading rates, shear-induced plasticity is observed. At rapid loading rates ($>100 \text{ mN s}^{-1}$), pressure-induced phase transformations are detected by *ex situ* micro-Raman spectroscopy and transmission electron microscopy. This switch in the deformation mechanism is due to the differing rate sensitivities of the respective deformation modes, shear-induced plasticity or pressure-induced phase transformation. © 2009 American Institute of Physics.

[DOI: 10.1063/1.3151967]

Under high hydrostatic pressures, open-structured covalent semiconductors such as Ge and Si exhibit a structural phase transformation to a dense, highly coordinated metallic phase. On pressure release these materials transform to complex crystalline structures that are metastable at ambient pressures. These transformed phases have novel electrical,¹ mechanical,² and chemical³ properties relative to the original (equilibrium) structure, giving them technological, as well as fundamental, significance.

Nanoindentation with a sharp diamond tip is a simple method for selectively inducing high-pressure phase transformation in a localized submicron region. In the case of Ge, however, there is some controversy as to whether a phase transformation can be induced via nanoindentation. The clearest evidence for an indentation-induced phase transformation in Ge has come from studies employing conventional microindenters, which have observed phase transformation by electrical resistance measurement⁴ and by micro-Raman spectroscopy.⁵ By contrast, several studies employing instrumented nanoindenters to study Ge have found any phase transformation to be weak or absent, and shear deformation by twinning and dislocation slip to instead be the dominant mechanism of deformation.^{6–8}

The inconsistency between these two sets of studies presumably stems from the difference in indentation (loading and/or unloading) conditions between conventional microindentation and instrumented nanoindentation systems. Apart from the maximum applied load, such an important difference is the rate of loading. In a nanoindentation test, this is typically $0.1\text{--}10 \text{ mN s}^{-1}$. For a microindenter the loading rate is typically orders of magnitude faster, $10\text{--}10^4 \text{ mN s}^{-1}$ depending on the instrument.⁹ In a previous study by Jang *et al.*,⁸ Ge was indented at loading rates of 0.5 and 5 mN s^{-1} .

There appeared to be a trend for phase transformations to be observed for the faster loading rate, but only reproducibly for a sharp cube-corner indenter, not for the more common Berkovich or spherical indenter geometries.

Phase transformation has also been observed after high-temperature indentation of Ge. Xiao and Pirouz¹⁰ observed formation of the hexagonal diamond Ge–V phase at the intersection of twin bands after high-temperature indentation of Ge. This was thought to be a means of accommodating the high strain at the intersection.

For this study, crystalline Ge (100) was indented using a Hysitron Triboindenter with a Berkovich tip, over a range of loading rates from 0.5 mN s^{-1} to 900 mN s^{-1} , up to 9 mN . Hardness values were obtained from nanoindentation *P-h* curves using Oliver and Pharr's¹¹ analysis.

Larger indents suitable for *ex situ* characterization were made using a UMIS-2000 nanoindenter, with a spherical ($R \approx 4.3 \text{ }\mu\text{m}$) tip and also with a Berkovich tip. Due to its method of load actuation, the UMIS instrument is normally capable of maximum loading rates of $\sim 10\text{--}20 \text{ mN s}^{-1}$. To obtain higher loading rates, tests were conducted in which the tip was rapidly brought in contact with the sample by manually lowering the indenter carriage. Applied force during this test was monitored and maximum load and loading rate determined from the load versus time trace. Loading rates of $100\text{--}200 \text{ mN s}^{-1}$ were typically obtained by this method.

Raman spectra were obtained from UMIS indents with a Renishaw 2000 micro-Raman instrument, using a 632.8 nm HeNe laser with a spot size of $\sim 1 \text{ }\mu\text{m}$ radius. Prior to measurements the instrument was calibrated to $\pm 1 \text{ cm}^{-1}$ on a clean silicon sample using the known Raman band position of Si–I. Laser power was kept low ($<100 \text{ }\mu\text{W}$) to avoid annealing any metastable phases. All spectra were collected more than a day after the indents were made.

^{a)}Electronic addresses: oliverd@mcgill.physics.ca and djo109@rsphysse.anu.edu.au.

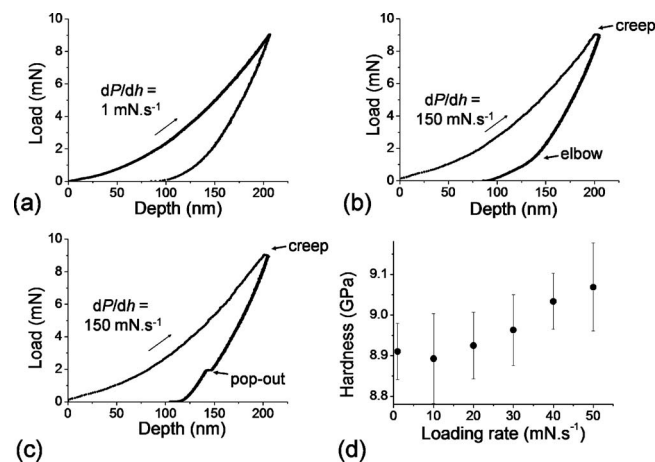


FIG. 1. P - h curves for Hysitron Berkovich indents to 9 mN at different loading rates: (a) 1 mN s^{-1} , (b) 150 mN s^{-1} , with elbow, and (c) 150 mN s^{-1} , with pop-out. For all curves the unloading rate is 10 mN s^{-1} . (d) Dependence of measured hardness on loading rate.

Cross-sections of indent damage were prepared for transmission electron microscope (TEM) examination using a focused ion beam system.⁷ Specimens were examined with a Philips CM 300 TEM.

P - h curves for Hysitron indents made at slow loading rates $< 50 \text{ mN s}^{-1}$ in Ge usually showed a classical elastic-plastic unloading response [Fig. 1(a)].¹¹ Indents at faster loading rates showed deviations from this behavior, notably some creep at maximum load (though no hold period was applied) and elbowing on unloading, as shown in Fig. 1(b). Some indents, as in Fig. 1(c), featured a pop-out displacement event on unloading, a feature that has been linked in Si to phase transformation.¹² Hardness values, plotted in Fig. 1(d), were found to increase with increasing loading rate.

For tests conducted using the UMIS at slow loading rates up to 15 mN s^{-1} , residual indents were found to contain no phase-transformed material. Representative Raman spectra are shown in Fig. 2(a). Spectra from slow loading rate indents featured only a single sharp Raman band at $305\text{--}310 \text{ cm}^{-1}$, corresponding to the Ge-I phase.

For UMIS indents made at loading rates $> 100 \text{ mN s}^{-1}$, additional phases were consistently visible in Raman spectra, as shown in Figs. 2(b) and 2(c). In addition to the Ge-I band, spectra contain a broad component below 290 cm^{-1} corresponding to amorphous Ge (a -Ge). Some indents featured several small peaks indicating the presence of an extra crystalline phase, as in Fig. 2(c), where peaks are observed at 153, 194, 217, 232, 251, and 280 cm^{-1} . These peak positions correspond to the positions previously observed for Ge-III,^{5,13} shifted upwards by $\sim 5 \text{ cm}^{-1}$. This shift is attributable to the influence of indentation-induced compressive stress on the Raman response.^{6,7} The relative intensities of the bands are roughly comparable to previously published spectra.⁵

The TEM micrograph in Fig. 3(a) shows the post-indentation damage observed in Ge for slow loading rates. A high density of shear defects is present. The inset dark-field image confirms the presence of shear-induced twin bands on $\{111\}$ planes.

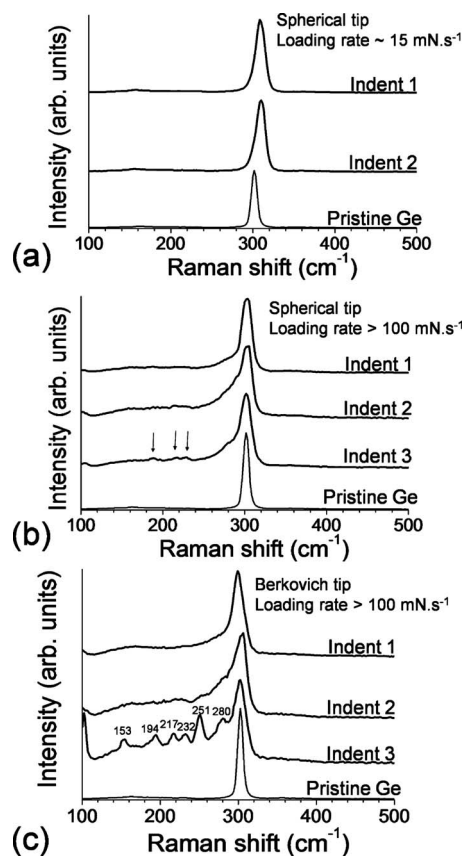


FIG. 2. Raman spectra for indents made to 100 mN maximum load: (a) slow loading rate ($\sim 15 \text{ mN s}^{-1}$), spherical tip, (b) rapid loading rate ($> 100 \text{ mN s}^{-1}$), spherical tip, (c) rapid loading rate ($> 100 \text{ mN s}^{-1}$), and Berkovich tip.

Figure 3(b) shows the nature of damage in Ge after rapid loading rate nanoindentation. Immediately below the surface there is a zone of transformed phase, recognizable by darker contrast. The SADP taken from this region [Fig. 3(c)] features reflections at $\sim 2.45 \text{ \AA}$ corresponding to the $\{211\}$ interplanar spacing of Ge-III, and reflections at $\sim 2.63 \text{ \AA}$ corresponding to the $\{201\}$, $\{112\}$ or $\{210\}$ spacings of Ge-III.¹⁴ In addition reflections corresponding to Ge-I and broad rings corresponding to a -Ge are present. Similar transformed zones were observed by cross-section TEM of other rapid loading rate indents. In some cases, only a -Ge was present.

The observations reported here clearly show phase transformations can be induced in Ge using both a Berkovich and spherical indenter. Indeed, unlike previous studies, Ge-III or a -Ge was consistently observed in rapid loading rate indents. The presence of Ge-III strongly indicates that the transformed material derives from a pressure-induced phase transition to metallic Ge-II (β -tin) under load, which transforms to Ge-III or a -Ge upon load release. Thus it appears that loading rate plays a critical role in determining whether a shear-induced or pressure-induced deformation mode operates. We will briefly outline a model to explain this result.

The strain rate sensitivity of the shear yield stress in Ge has been investigated by several groups,¹⁵ and the yield stress has been found to increase with strain rate. Plasticity under nanoindentation at room temperature clearly falls into the “low temperature, high stress” regime,¹⁶ in which twin-

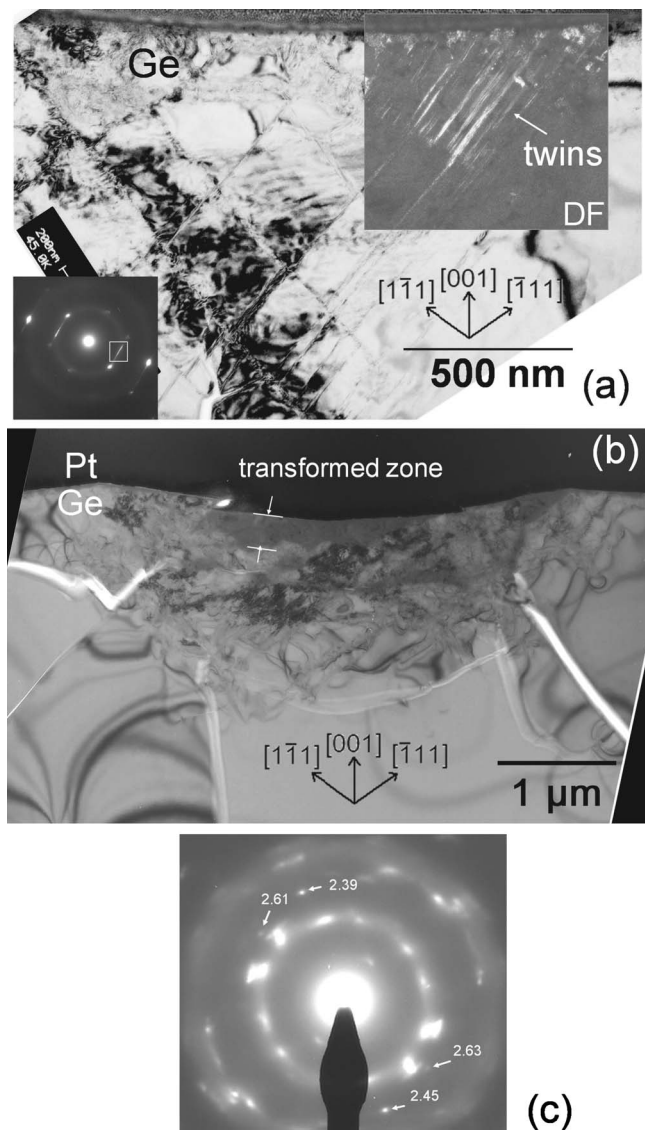


FIG. 3. (a) Bright-field (BF) $\langle 110 \rangle$ zone axis TEM micrograph of slow loading rate spherical indent to a maximum load of 50 mN at a loading rate of $\sim 1 \text{ mN s}^{-1}$. Inset: dark-field image taken with the boxed reflection in the diffraction pattern (lower left inset). (b) BF $\langle 110 \rangle$ zone axis TEM micrograph of rapid loading rate spherical indent to $\sim 80 \text{ mN}$, at $\sim 165 \text{ mN s}^{-1}$. (c) SADP taken from phase-transformed region in (b).

ning is the dominant shear mechanism. According to the model proposed by Pirouz,¹⁷ this depends upon thermally activated cross-slip for twin growth. Twinning can thus be expected to show a strong dependence on the strain rate: in other words, the critical shear stress for twinning will increase as loading rate increases. This is consistent with the observed increase in hardness with loading rate [Fig. 1(d)].

The β -tin phase transformation is much less strain rate sensitive. Shock loading experiments have been carried out on silicon with pressure increase rates greater than 10^7 GPa s^{-1} .¹⁸ The β -tin transition was observed in that experiment at $\sim 11 \text{ GPa}$, not significantly different from the transition pressure of 12.5 GPa observed in diamond-anvil cell experiments¹⁹ (in which typical loading rates are $< 1 \text{ GPa min}^{-1}$). Thus over a very large loading rate range,

the diamond-cubic $\rightarrow \beta$ -tin transition appears to be relatively rate-insensitive.

The ratio of shear to hydrostatic stresses during initial (elastic) indentation is determined by the indenter geometry. Since the critical stress required for shear plasticity rises with increased loading rate, while the stress for phase transition remains unchanged, this implies a threshold loading rate exists, above which phase transition becomes a favorable response. This is entirely consistent with our experimental observations.

In the light of these results, the inconsistency between studies conducted using high-load conventional microindentation and studies conducted with instrumented nanoindentation can be explained. The loading rate in a Vickers microindentation test varies depending on the instrument, but is generally greater than 10 mN s^{-1} and may be as high as 10^4 mN s^{-1} .⁹ Most Vickers tests then would be in a loading regime where shear plasticity is rate-limited, and phase transformation consequently favorable.

The ability to induce phase transformation in Ge by nanoindentation opens up similar technological possibilities as have been proposed for Si.⁵ Furthermore, we predict similar indentation rate sensitivity in other open-structured covalent materials, such as III-V and II-VI semiconductors. Shear-induced twinning and slip are observed under indentation for GaAs and other compound semiconductors,^{20,21} and shear mechanisms in these materials are rate-limited as in Ge.

¹S. Ruffell, J. E. Bradby, N. Fujisawa, and J. S. Williams, *J. Appl. Phys.* **101**, 083531 (2007).

²I. Zarudi, L. C. Zhang, and M. V. Swain, *Appl. Phys. Lett.* **82**, 1027 (2003).

³R. Rao, J. E. Bradby, and J. S. Williams, *Appl. Phys. Lett.* **91**, 123113 (2007).

⁴D. R. Clarke, M. C. Kroll, P. D. Kirchner, R. F. Cook, and B. J. Hockey, *Phys. Rev. Lett.* **60**, 2156 (1988).

⁵A. Kailer, K. G. Nickel, and Y. G. Gogotsi, *J. Raman Spectr.* **30**, 939 (1999).

⁶Y. G. Gogotsi, V. Domnich, S. N. Dub, A. Kailer, and K. G. Nickel, *J. Mater. Res.* **15**, 871 (2000).

⁷J. E. Bradby, J. S. Williams, J. Wong-Leung, M. V. Swain, and P. Munroe, *Appl. Phys. Lett.* **80**, 2651 (2002).

⁸J. Jang, M. J. Lance, S. Wen, and G. M. Pharr, *Appl. Phys. Lett.* **86**, 131907 (2005).

⁹G. D. Quinn, P. J. Patel, and I. Lloyd, *J. Res. Natl. Inst. Stand. Technol.* **107**, 299 (2002).

¹⁰S.-Q. Xiao and P. Pirouz, *J. Mater. Res.* **7**, 1406 (1992).

¹¹W. Oliver and G. Pharr, *J. Mater. Res.* **7**, 1564 (1992).

¹²V. Domnich, Y. Gogotsi, and S. N. Dub, *Appl. Phys. Lett.* **76**, 2214 (2000).

¹³R. J. Kobliska, S. A. Solin, M. Selders, R. K. Chang, R. Alben, M. F. Thorpe, and D. Weaire, *Phys. Rev. Lett.* **29**, 725 (1972).

¹⁴J. S. Kasper and S. M. Richards, *Acta Crystallogr.* **17**, 752 (1964).

¹⁵H. Siethoff, K. Ahlborn, and W. Schroter, *Phys. Status Solidi A* **174**, 205 (1999).

¹⁶P. Pirouz, A. V. Samant, M. H. Hong, A. Moulin, and L. P. Kubin, *J. Mater. Res.* **14**, 2783 (1999).

¹⁷P. Pirouz and P. M. Hazzledine, *Scr. Metall. Mater.* **25**, 1167 (1991).

¹⁸H. Kishimura and H. Matsumoto, *J. Appl. Phys.* **103**, 023505 (2008).

¹⁹J. Z. Hu, L. D. Merkle, C. S. Menoni, and I. L. Spain, *Phys. Rev. B* **34**, 4679 (1986).

²⁰J. E. Bradby, J. S. Williams, J. Wong-Leung, M. V. Swain, and P. Munroe, *Appl. Phys. Lett.* **78**, 3235 (2001).

²¹J. E. Bradby, S. O. Kucheyev, J. S. Williams, C. Jagadish, M. V. Swain, P. Munroe, and M. R. Phillips, *Appl. Phys. Lett.* **80**, 4537 (2002).